https://doi.org/10.15407/ujpe67.12.859

A.V. KOROTUN [1, 2]

[1] National University "Zaporizhzhia Polytechnic"
(64, Zhukovs'kogo Str., Zaporizhzhya 69063, Ukraine; e-mail: andko@zp.edu.ua)
[2] G.V. Kurdyumov Institute for Metal Physics, Nat. Acad. of Sci. of Ukraine
(36, Akademika Vernads'kogo Blvd., Kyiv 03142, Ukraine)

POLARIZABILITY OF A HEMISPHERICAL METAL NANOPARTICLE LOCATED ON A DIELECTRIC SUBSTRATE

The frequency dependence of the dipole polarizability has been determined in the quadrupole approximation for a metal hemisphere located on a dielectric substrate in the case where light is normally incident on the substrate. Formulas for the effective relaxation time and for the invisibility and surface plasmon resonance frequencies are obtained. The evolution of plasmon resonances with a change in the hemisphere radius is studied. The origin of two resonances in the imaginary part of the polarizability and the difference of the maxima in the imaginary part of the polarizability of the hemispheres made of different metals are discussed. The character and position of the resonances in the imaginary part of the polarizability of aluminum islands are explained. Recommendations regarding the creation of an invisibility frequency band near the metal nanoisland are given.

K e y w o r d s: metal hemisphere, polarizability, surface plasmon resonance, invisibility frequency, quadrupole approximation.

1. Introduction

The rapid development of nanotechnology in recent decades stimulated the emergence of nanoplasmonics [1–9], which is an area located at the intersection of optics and materials science, and which studies optical phenomena in solid-state nanostructures. One of the phenomena appearing when light interacts with surfaces or structures whose sizes are smaller than the light wavelength is the localized surface plasmon resonance (SPR) [1, 2, 5, 6, 8–13]. This unique phenomenon, in turn, leads to the strong localization of photons at the nanoscale level and allows such structures to be applied in advanced nanophotonic technologies [4, 6, 7, 14–17].

A special case of metal nanostructures, which are of considerable practical interest, are metal island films [18–20]. Such systems open wide prospects for the development of spectrally selective absorbing coatings [21], devices for enhanced fluorescence and infrared spectroscopy [22, 23], polarizers and spectral filters [24], methods of invasive optical sensing and cancer therapy [7], as well as spectroscopic diagnostic studies including surface-enhanced Raman scattering (SERS) [25, 26]. In addition, separate islands and their groups can be used to represent information units, which allows the development of methods for optical data storage with an ultrahigh recording density, an extremely long data storage life, and an ultralow power consumption [27, 28]. Advanced techniques for transferring metal nanoislands onto a flexible substrate, such as polymethylsiloxane [29, 30], open up opportunities for creating a new generation of devices in such domains as medical diagnostics, food safety, and environmental monitoring.

An important characteristic governing the optical properties of nanostructures is their polarizability, i.e., the ability of an electron cloud to change its shape under the influence of an external field. The frequencies of localized surface plasmons are known to correspond to polarizability resonances, whereas the invisibility frequencies to zero polarizability and, accordingly, the absence of scattering. Therefore, by calculating the polarizability of the system, it is possible to find the SPR frequencies and the invisibility ones.

When studying the influence of the shape of metal nanoparticles on their optical properties, the authors of a number of theoretical works assumed that

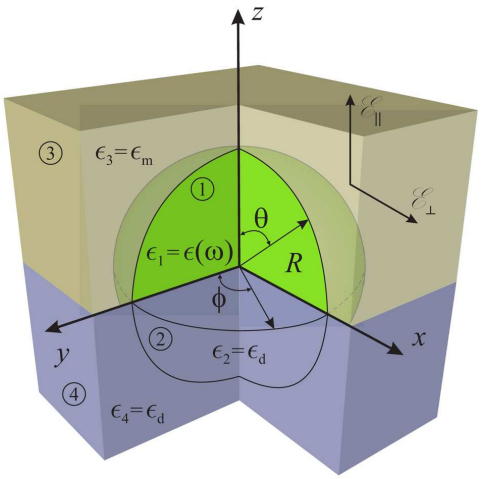

Fig. 1. Schematic diagram of a hemisphere on a substrate

the dissipative processes inside the nanoparticle are characterized by the scalar high-frequency conductivity. However, as was shown in works [31–33], if the particle sizes are smaller than the electron free path length, and if the particles are non-spherical in shape, the optical conductivity becomes a tensor quantity, and electron scattering at the nanoparticle surface is substantial and must be taken into account. Furthermore, as was shown in works [34, 35], the role of another dissipation channel increases with the growth of the particle size; this is radiation damping, and analytical expressions were derived for its relaxation rate in the cases of spherical and ellipsoidal nanoparticles. Expressions obtained in this theory were adapted for metal nanocylinders and nanodisks (see works [36, 37]), as well as for layered spherical nanoparticles [38, 39]. However, the issue concerning the relaxation mechanisms in metal islands on dielectric substrates has not been studied yet.

Note that if nanoparticles are sufficiently large, higher multipole resonances can play a substantial role. Therefore, the analysis of the quadrupole contribution to the dipole polarizability is also pertinent.

Since metal islands are usually obtained in experiments in the form of hemispheres [40], the purpose of this work is to calculate the polarizability of metal hemispheres located on a dielectric substrate accounting simultaneously for the influence of the surface and the radiation damping, as well as the quadrupole contribution to the dipole polarizability. Another aim consists in obtaining and analyzing expressions for the SPR and invisibility frequencies.

2. Basic Relations

2.1. Polarizability of hemispherical nanoparticle

Consider a metal nanoisland (medium *1*) in the form of a hemisphere with the radius R and the dielectric permittivity $\epsilon(\omega)$ (see Fig. 1). The hemisphere is located on a dielectric substrate with the dielectric permittivity $\epsilon_{\rm d}$ (medium *2*). The dielectric permittivity of the environment equals $\epsilon_{\rm m}$ (medium *3*). Auxiliary region *4* in the substrate has the dielectric permittivity $\epsilon_{\rm d}$ (medium *4*).

Owing to the system anisotropy, there are two independent solutions: for the external field $\mathcal{E}$ directed perpendicularly or in parallel to the substrate plane (Fig. 1). Therefore, there are two independent diagonal components in the polarizability tensor of the hemispherical metal nanoparticle: the longitudinal one, $\alpha_\parallel$, corresponding to the external field directed perpendicularly to the substrate and in parallel to the Oz axis ($\mathcal{E} \parallel Oz$); and the transverse one, $\alpha_\perp$, when the external field is parallel to the substrate and perpendicular to the axis Oz ($\mathcal{E} \perp Oz$). The latter case corresponds to normal light incidence. Since this geometry is most often realized in plasmon experiments, we consider the situation when the external field is directed in parallel to the substrate and perpendicularly to the Oz axis.

If the size of the nanoparticle is much smaller than the light wavelength, the quasistatic approximation can be used to solve the problem. In this case, the potential created by the hemisphere in the whole space is described by the solutions of the Laplace equation

$$\Delta\varphi = 0 \tag{1}$$

with the corresponding boundary conditions, namely, the continuity of the potential and the normal component of the electric induction vector across the interfaces between the hemispheres and the half-spaces (medium *1*-medium *3* and medium *2*-medium *4*),

$$\begin{aligned}
&\varphi_1|_{r=R} = \varphi_3|_{r=R};\\
&\varphi_2|_{r=R} = \varphi_4|_{r=R};\\
&\epsilon(\omega)\left.\frac{\partial\varphi_1}{\partial r}\right|_{r=R} = \epsilon_{\rm m}\left.\frac{\partial\varphi_3}{\partial r}\right|_{r=R};\\
&\left.\frac{\partial\varphi_2}{\partial r}\right|_{r=R} = \left.\frac{\partial\varphi_4}{\partial r}\right|_{r=R};
\end{aligned} \tag{2}$$

and across the flat interfaces between the hemispheres (medium *1*-medium *2*) and between the half-spaces (medium *3*-medium *4*),

$$\begin{aligned}
&\varphi_1|_{\theta=\frac{\pi}{2}} = \varphi_2|_{\theta=\frac{\pi}{2}};\\
&\varphi_3|_{\theta=\frac{\pi}{2}} = \varphi_4|_{\theta=\frac{\pi}{2}};\\
&\epsilon\,(\omega)\,\frac{\partial\varphi_1}{\partial\theta}\bigg|_{\theta=\frac{\pi}{2}} = \epsilon_{\rm d}\,\frac{\partial\varphi_2}{\partial\theta}\bigg|_{\theta=\frac{\pi}{2}};\\
&\epsilon_{\rm m}\frac{\partial\varphi_3}{\partial\theta}\bigg|_{\theta=\frac{\pi}{2}} = \epsilon_{\rm d}\,\frac{\partial\varphi_4}{\partial\theta}\bigg|_{\theta=\frac{\pi}{2}}.
\end{aligned} \tag{3}$$

In the general case, the solutions of Eq. (1) for the potentials inside and outside the hemisphere in the dipole approximation have the form

$$\begin{cases}
\varphi_1 = Ar\sin\theta\cos\phi,\\
\varphi_2 = \left(\dfrac{B}{r^2} - C\mathcal{E}_0 r\right)\sin\theta\cos\phi,\\
\varphi_3 = \left(\dfrac{D}{r^2} - \mathcal{E}_0 r\right)\sin\theta\cos\phi,\\
\varphi_4 = \mathcal{E}_0 r\sin\theta\cos\phi,
\end{cases} \tag{4}$$

where ϕ is the polar angle, θ is the azimuthal angle, r is the radial coordinate, and the constants A, B, C, and D are determined by the boundary conditions.

Substituting Eqs. (4) into Eqs. (2) and (3), we obtain

$$AR = \frac{D}{R^2} - \mathcal{E}_0 R;$$

$$ER = \frac{B}{R^2} - C\mathcal{E}_0 R;$$

$$A\epsilon\,(\omega) = -\left(\frac{2D}{R^3} + \mathcal{E}_0\right)\epsilon_m;$$

$$E = -\frac{2B}{R^3} - C\mathcal{E}_0;$$

whence

$$\alpha^{\perp}_{\rm dip} = \frac{D}{\mathcal{E}_0 R^3} = \frac{\epsilon^{\perp}\,(\omega) - \epsilon_m}{\epsilon^{\perp}(\omega) + 2\epsilon_m}. \tag{5}$$

Here, the Drude dielectric function is used for the metal,

$$\epsilon^{\perp}\,(\omega) = \epsilon^{\infty} - \frac{\omega_p^2}{\omega^2 + \left(\tau^{\perp}_{\rm eff}\right)^{-2}} + {\rm i}\frac{\omega_p^2}{\omega\left[\omega^2 + \left(\tau^{\perp}_{\rm eff}\right)^{-2}\right]}, \tag{6}$$

where $\omega_p = \sqrt{e^2 n_e/\epsilon_0 m^*}$ is the plasma frequency; e and n_e are the electron charge and concentration, respectively; $n_e = 3/(4\pi r_s^3)$; r_s is the average distance between the electrons; ϵ_0 is the electric constant; m^* is the effective electron mass; ϵ^{∞} is the contribution of the ionic core to the dielectric permittivity; and $\left(\tau^{\perp}_{\rm eff}\right)^{-1}$ is the transverse component of the inverse tensor of the effective relaxation time. The latter parameter is determined via the inverse times of the bulk and surface relaxations and the radiation damping as follows:

$$\frac{1}{\tau^{\perp}_{\rm eff}} = \frac{1}{\tau_{\rm bulk}} + \frac{1}{\tau^{\perp}_{\rm surf}} + \frac{1}{\tau^{\perp}_{\rm rad}}. \tag{7}$$

The tensor character of the inverse effective relaxation time and its components is associated with the system anisotropy. The latter manifests itself in that the optical response of the nanosystem is different in the cases where the external electric field $\mathcal{E}_0$ is parallel or perpendicular to the dielectric substrate.

The relationships for the transverse components of the tensors of the inverse surface relaxation times and radiation damping for a hemispherical nanoparticle can be written in the form [12]

$$\frac{1}{\tau^{\perp}_{\rm surf}} = \frac{\mathcal{L}_{\perp}{\rm Re}\,\sigma_{\perp}}{\epsilon_0\left[\epsilon_{\rm m} + \mathcal{L}_{\perp}\,(1-\epsilon_{\rm m})\right]}, \tag{8}$$

$$\frac{1}{\tau^{\perp}_{\rm rad}} = \frac{V}{6\pi\epsilon_0}\left(\frac{\omega_p}{c}\right)^3 \frac{\mathcal{L}_{\perp}{\rm Re}\,\sigma_{\perp}}{\sqrt{\epsilon_{\rm m}\left[\epsilon^{\infty} + \left(\dfrac{1}{\mathcal{L}_{\perp}} - 1\right)\epsilon_{\rm m}\right]}}, \tag{9}$$

where c is the speed of light, $V = 2\pi R^3/3$ is the nanoparticle volume, $\mathcal{L}_{\perp}$ is the depolarization factor, and $\sigma_{\perp}$ is the transverse component of the conductivity tensor.

Substituting expressions (8) and (9) in formula (7), we obtain

$$\frac{1}{\tau^{\perp}_{\rm eff}} = \frac{1}{\tau_{\rm bulk}} + \left\{\frac{1}{\epsilon_{\rm m} + \mathcal{L}_{\perp}\,(1-\epsilon_{\rm m})} + \frac{V}{6\pi}\left(\frac{\omega_p}{c}\right)^3 \times \right.$$

$$\left. \times \frac{1}{\sqrt{\epsilon_{\rm m}\left[\epsilon^{\infty} + \left(\frac{1}{\mathcal{L}_{\perp}} - 1\right)\epsilon_{\rm m}\right]}}\right\}\frac{\mathcal{L}_{\perp}}{\epsilon_0}\,{\rm Re}\,\sigma_{\perp}, \tag{10}$$

where ${\rm Re}\,\sigma_{\perp}$ does not differ from the corresponding quantity for the spherical nanoparticle, i.e., it looks like [41]

$${\rm Re}\,\sigma_{\perp} = {\rm Re}\,\sigma_{\rm sph} = \frac{3\epsilon_0}{2}\nu_s\left(\frac{\omega_p}{\omega}\right)^2 \times$$

$$\times \left[1 - \frac{2\nu_s}{\omega}\sin\frac{\omega}{\nu_s} + \frac{2\nu_s^2}{\omega^2}\left(1 - \cos\frac{\omega}{\nu_s}\right)\right], \quad (11)$$

where $\nu_s = v_{\rm F}/(2R)$ is the frequency of individual oscillations, and $v_{\rm F}$ is the Fermi velocity of electrons.

Let us determine the depolarization factors $\mathcal{L}_{\perp(\parallel)}$. According to the general formula [42],

$$\mathcal{L}_{\parallel} = \frac{1}{4\pi}\int\limits_S \frac{[\mathbf{r},\mathbf{n}]_z}{r^3}dS, \quad (12)$$

where $\mathbf{n}$ is the vector normal to the hemisphere surface, $\mathbf{r}$ is the radius vector, and the integration is performed over the hemisphere's surface. Calculating the integral in the spherical coordinate system, we get

$$\mathcal{L}_{\parallel} = \frac{1}{4\pi}\int\limits_S \frac{r}{r^3}r^2\sin\theta d\theta d\varphi =$$

$$= \frac{1}{4\pi}\int\limits_0^{2\pi} d\varphi \int\limits_0^{\frac{\pi}{2}} \sin\theta d\theta = \frac{1}{2}. \quad (13)$$

Taking into account that the depolarization factors satisfy the relation $2\mathcal{L}_\perp + \mathcal{L}_\parallel = 1$, we obtain that $\mathcal{L}_\perp = 1/4$ for hemispherical islands. Substituting this expressions for $\mathcal{L}_\perp$ and expression (11) for Re $\sigma_\perp$ in formula (10), we obtain the final expression for the inverse transverse effective relaxation time,

$$\frac{1}{\tau_{\rm eff}^{\perp}} = \frac{1}{\tau_{\rm bulk}} + \frac{3}{8}\nu_s\left(\frac{\omega_p}{\omega}\right)^2 \times$$

$$\times \left[\frac{4}{3\epsilon_{\rm m}+1} + \frac{V}{6\pi}\left(\frac{\omega_p}{c}\right)^3 \frac{1}{\sqrt{\epsilon_{\rm m}\left[3\epsilon_{\rm m}+\epsilon^{\infty}\right]}}\right] \times$$

$$\times \left[1 - \frac{2\nu_s}{\omega}\sin\frac{\omega}{\nu_s} + \frac{2\nu_s^2}{\omega^2}\left(1 - \cos\frac{\omega}{\nu_s}\right)\right]. \quad (14)$$

Note that expression (14) describes the frequency dependence of the effective electron relaxation time in a hemispherical metal island with a fixed size.

Thus, in the dipole approximation, the formulas for the polarizability of a homogeneous spherical nanoparticle and a hemispherical nanoparticle on a substrate formally coincide, although $\epsilon_{\rm semisph}(\omega) \neq \neq \epsilon_{\rm sph}(\omega)$ owing to different values of the inverse effective relaxation times.

Now, let us obtain an expression for the dipole polarizability in the quadrupole approximation. The corresponding solutions of the Laplace equation in media *1*, *2*, *3*, and *4* look like

$$\varphi_1 = \left[A_1 r P_1^1(\cos\theta) + A_2 r^2 P_2^1(\cos\theta)\right]\cos\phi, \quad (15)$$

$$\varphi_2 = \left[\frac{B_1}{r^2}P_1^1(\cos\theta) + \right.$$

$$\left. + \frac{B_2}{r^3}P_2^1(\cos\theta) - \mathcal{E}_0 r P_1^1(\cos\theta)\right]\cos\phi, \quad (16)$$

$$\varphi_3 = \left[\frac{C_1}{r^2}P_1^1(\cos\theta) + \right.$$

$$\left. + \frac{C_2}{r^3}P_2^1(\cos\theta) - \mathcal{E}_0 r P_1^1(\cos\theta)\right]\cos\phi, \quad (17)$$

$$\varphi_4 = \left[D_1 r P_1^1(\cos\theta) + D_2 r^2 P_2(\cos\theta)\right]\cos\phi, \quad (18)$$

where the explicit expressions for the required Legendre polynomials are as follows [43]:

$$P_1^1(\cos\theta) = \sin\theta, \quad (19)$$

$$P_2^1(\cos\theta) = \frac{3}{2}\sin 2\theta = 3\sin\theta\cos\theta. \quad (20)$$

Then, the expression for the dimensionless transverse component of the dipole polarizability tensor, in which the dipole and quadrupole contributions are taken into account, has the form (see Appendix)

$$\tilde{\alpha}_{\rm q}^{\perp} = \frac{\Lambda}{\Xi}, \quad (21)$$

where the following notations were introduced:

$$\Lambda = (\epsilon_{\rm d} + 5\epsilon_{\rm m})\epsilon^2(\omega) +$$

$$+ (3\epsilon_{\rm d} + 5\epsilon_{\rm m})\epsilon_{\rm m}\epsilon(\omega) - 4\epsilon_{\rm d}\epsilon_{\rm m}^2, \quad (22)$$

$$\Xi = (4\epsilon_{\rm d} + 5\epsilon_{\rm m})\epsilon^2(\omega) +$$

$$+ 2\left(3\epsilon_{\rm d}^2 + 5\epsilon_{\rm m}^2 + 9\epsilon_{\rm d}\epsilon_{\rm m}\right)\epsilon(\omega) +$$

$$+ 2\epsilon_{\rm d}\epsilon_{\rm m}(3\epsilon_{\rm d} + 4\epsilon_{\rm m}). \quad (23)$$

Relations (5) and (21)–(23), as well as expressions (6) and (14), are used below to calculate the frequency dependences of the transverse component of the polarizability tensor in the dipole and quadrupole approximations.

2.2. Invisibility and surface plasmon resonance frequencies

Let the imaginary part of the dielectric function be much smaller than the real part, and $\omega\tau_{\text{eff}}^{\perp} \gg 1$. Then, expression (6) takes the form

$$\epsilon(\omega) = \epsilon^{\infty} - \frac{\omega_p^2}{\omega^2}. \tag{24}$$

By factorizing the numerator and denominator in expression (21)

$$\tilde{\alpha}_{\perp} = \frac{\left(\epsilon(\omega) - \tilde{\epsilon}^{(+)}\right)\left(\epsilon(\omega) - \tilde{\epsilon}^{(-)}\right)}{\left(\epsilon(\omega) - \epsilon^{(+)}\right)\left(\epsilon(\omega) - \epsilon^{(-)}\right)}, \tag{25}$$

putting $\epsilon(\omega) = \epsilon^{(\pm)}$, and substituting in formula (24), we obtain the following expression for the surface plasmon frequencies:

$$\omega_{\text{sp}}^{(\pm)} = \frac{\omega_{\text{p}}}{\sqrt{\epsilon^{\infty} - \epsilon^{(\pm)}}}, \tag{26}$$

where

$$\epsilon^{(\pm)} = \frac{-3\epsilon_d^2 - 9\epsilon_d\epsilon_{\text{m}} - 5\epsilon_{\text{m}}^2}{4\epsilon_d + 5\epsilon_{\text{m}}} \pm$$
$$\pm \frac{\sqrt{9\epsilon_d^4 + 30\epsilon_d^3\epsilon_{\text{m}} + 49\epsilon_d^2\epsilon_{\text{m}}^2 + 50\epsilon_d\epsilon_{\text{m}}^3 + 25\epsilon_{\text{m}}^4}}{4\epsilon_d + 5\epsilon_{\text{m}}}. \tag{27}$$

Let $\epsilon^{\infty} = \epsilon_{\text{m}} = 1$. Then,

$$\epsilon^{(\pm)} = \frac{1}{4\epsilon_d + 5}\Big(-3\epsilon_d^2 - 9\epsilon_d - 5 \pm$$
$$\pm \sqrt{9\epsilon_d^4 + 30\epsilon_d^3 + 49\epsilon_d^2 + 50\epsilon_d + 25}\Big), \tag{28}$$

and the splitting of the SPR frequencies equals

$$\Delta\omega_{\text{sp}} = \omega_{\text{sp}}^{(+)} - \omega_{\text{sp}}^{(-)} =$$
$$= \omega_{\text{p}}\left(\frac{1}{\sqrt{1 - \epsilon^{(+)}}} - \frac{1}{\sqrt{1 - \epsilon^{(-)}}}\right). \tag{29}$$

The invisibility condition is obtained by zeroing the numerator in expression (25), i.e., by putting

$$\epsilon\left(\omega^{\#}\right) = \tilde{\epsilon}^{(\pm)}, \tag{30}$$

where

$$\omega^{\#(\pm)} = \frac{\omega_{\text{p}}}{\sqrt{\epsilon^{\infty} - \tilde{\epsilon}^{(\pm)}}} \tag{31}$$

and

$$\tilde{\epsilon}^{(\pm)} = \frac{-\epsilon_{\text{m}}(3\epsilon_d + 5\epsilon_{\text{m}})}{2(\epsilon_d + 5\epsilon_{\text{m}})} \pm$$
$$\pm \frac{\epsilon_{\text{m}}\sqrt{5(5\epsilon_d^2 + 27\epsilon_d\epsilon_{\text{m}} + 5\epsilon_{\text{m}}^2)}}{2(\epsilon_d + 5\epsilon_{\text{m}})}. \tag{32}$$

Let $\epsilon^{\infty} = \epsilon_{\text{m}} = 1$. Then we have

$$\tilde{\epsilon}^{(\pm)} = \frac{-3\epsilon_d - 5 \pm \sqrt{5(5\epsilon_d^2 + 27\epsilon_d + 5)}}{2(\epsilon_d + 5)}, \tag{33}$$

and the difference between the invisibility frequencies equals

$$\Delta\omega^{\#} = \omega^{\#(+)} - \omega^{\#(-)} =$$
$$= \omega_{\text{p}}\left(\frac{1}{\sqrt{1 - \tilde{\epsilon}^{(+)}}} - \frac{1}{\sqrt{1 - \tilde{\epsilon}^{(-)}}}\right). \tag{34}$$

Relations (26), (28), (29), (31), (33), and (34) are used below to calculate the invisibility and SPR frequencies, as well as their splitting.

3. Calculation Results and Their Discussion

Specific calculations were carried out for Al, Cu, Au, Ag, Pt, and Pd nanoislands located on a glass substrate ($\epsilon_{\text{d}} = 2.25$) and in various environments. The parameters of metals and matrices are quoted in Tables 1 and 2, respectively.

Figure 2 demonstrates the frequency dependences of the real and imaginary parts of the transverse component of the polarizability tensor for Au hemispheres of various sizes, which were calculated in the dipole approximation. Note that $\text{Re}\,\tilde{\alpha}_{\text{dip}}^{\perp}(\hbar\omega)$ is a sign-changing function of the frequency (Fig. 2, *a*), whereas $\text{Im}\,\tilde{\alpha}_{\text{dip}}^{\perp}(\hbar\omega) > 0$ in the whole examined frequency interval (Fig. 2, *b*). In addition, as the size

Table 1. **Parameters of metals (see, e.g., works [36, 37] and references therein)**

Parameter	Al	Cu	Au	Ag	Pt	Pd
r_s/a_0	2.07	2.11	3.01	3.02	3.27	4.00
m^*/m_e	1.06	1.49	0.99	0.96	0.54	0.37
ϵ^{∞}	0.7	12.03	9.84	3.7	4.42	2.52
τ_{bulk}, fs	8	27	29	40	9.5	7.2

Table 2. **Dielectric permittivities of matrices [44]**

Matrix	Air	CaF_2	Teflon	TiO_2	C_{60}
ϵ_m	1	1.54	2.3	4.0	6.0

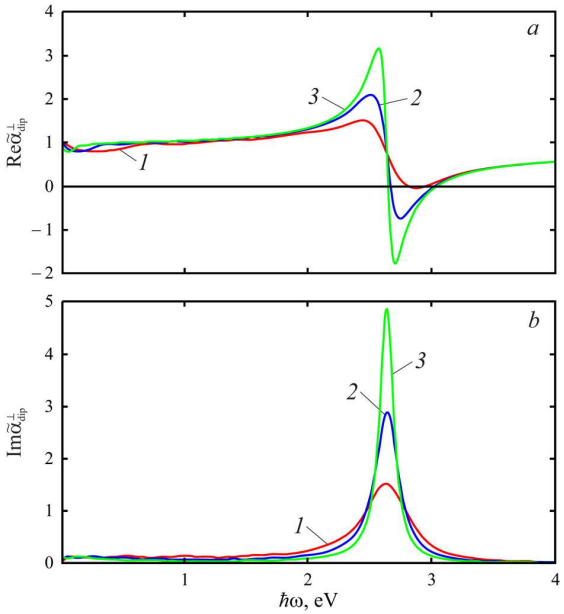

Fig. 2. Frequency dependences of the real and imaginary parts of the transverse component of the polarizability tensor calculated in the dipole approximation for Au hemispheres of various radii $R = 10$ (*1*), 20 (*2*), and 50 nm (*3*)

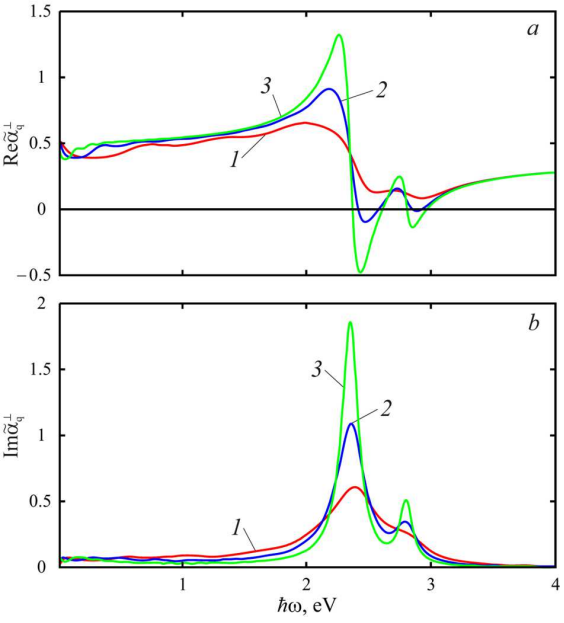

Fig. 3. The same dependences as in Fig. 2, but calculated in the quadrupole approximation. The environment is air

of nanoislands increases, the absolute values of the minima and maxima in $\mathrm{Re}\,\tilde{\alpha}^{\perp}_{\mathrm{dip}}(\hbar\omega)$ and the maxima in $\mathrm{Im}\,\tilde{\alpha}^{\perp}_{\mathrm{dip}}(\hbar\omega)$ grow. Such a behavior of the functions $\mathrm{Re}\,\tilde{\alpha}^{\perp}_{\mathrm{dip}}(\hbar\omega)$ and $\mathrm{Im}\,\tilde{\alpha}^{\perp}_{\mathrm{dip}}(\hbar\omega)$ is similar to that of the functions $\mathrm{Re}\,\tilde{\alpha}_{\mathrm{dip}}(\hbar\omega)$ and $\mathrm{Im}\,\tilde{\alpha}_{\mathrm{dip}}(\hbar\omega)$ for the metal ball.

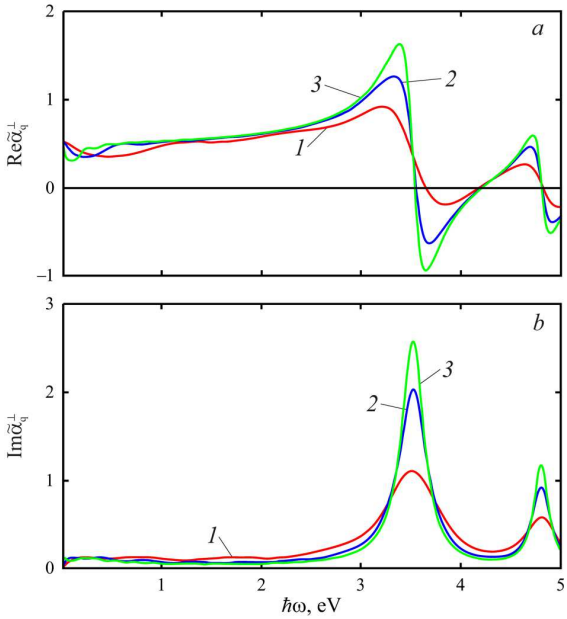

Fig. 4. The same as in Fig. 4 but for Pt nanoislands

The calculation results obtained for the frequency dependences of the real and imaginary parts of the transverse polarizability component in the quadrupole approximation for Au nanoislands are shown in Fig. 3. The numbers of minima and maxima and their values for $\mathrm{Re}\,\tilde{\alpha}^{\perp}_{\mathrm{q}}$ and $\mathrm{Im}\,\tilde{\alpha}^{\perp}_{\mathrm{q}}$ depend substantially on the island radius R. In particular, the number of extrema and their absolute values increase with the growth of R. For the island radius $R = 10$ nm, the curves $\mathrm{Re}\,\tilde{\alpha}^{\perp}_{\mathrm{q}}$ have one maximum and one minimum (Fig. 3 *a*), and the curves $\mathrm{Im}\,\tilde{\alpha}^{\perp}_{\mathrm{q}}$ have one maximum (Fig. 3, *b*). As the radius grows (curves *2* and *3* in Fig. 3), there arise additional extrema in the dependencies $\mathrm{Re}\,\tilde{\alpha}^{\perp}_{\mathrm{q}}(\hbar\omega)$ and $\mathrm{Im}\,\tilde{\alpha}^{\perp}_{\mathrm{q}}(\hbar\omega)$, and the first minimum of $\mathrm{Re}\,\tilde{\alpha}^{\perp}_{\mathrm{q}}$ corresponds to the first maximum of $\mathrm{Im}\,\tilde{\alpha}^{\perp}_{\mathrm{q}}(\hbar\omega)$. The maxima of the imaginary part of the polarizability correspond to the surface plasmon resonance, and the presence of two peaks is associated with the dipole and quadrupole contributions.

The frequency dependences of the real and imaginary parts of the transverse polarizability component for Pt nanoislands (Fig. 4) are qualitatively similar to their counterparts for Au nanoislands, but the ab-

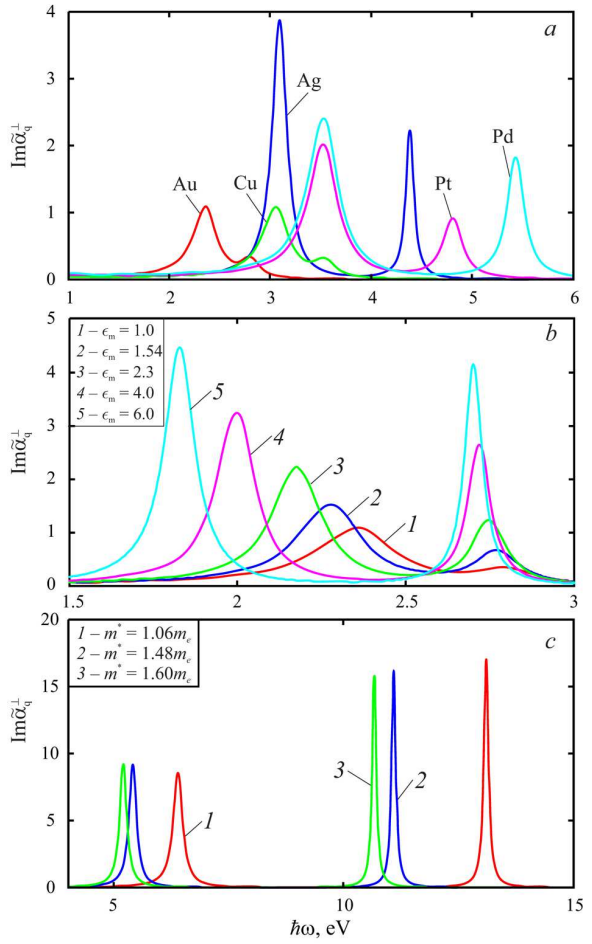

Fig. 5. Frequency dependences of the imaginary part of the transverse component of the polarizability tensor for (*a*) nanoislands of various metals, (*b*) Au nanoislands in various environments, and (*c*) Al nanoislands with various effective electron masses. In all cases, the environment is air ($\epsilon_{\rm m} = 1$) and the nanoisland radius $R = 20$ nm

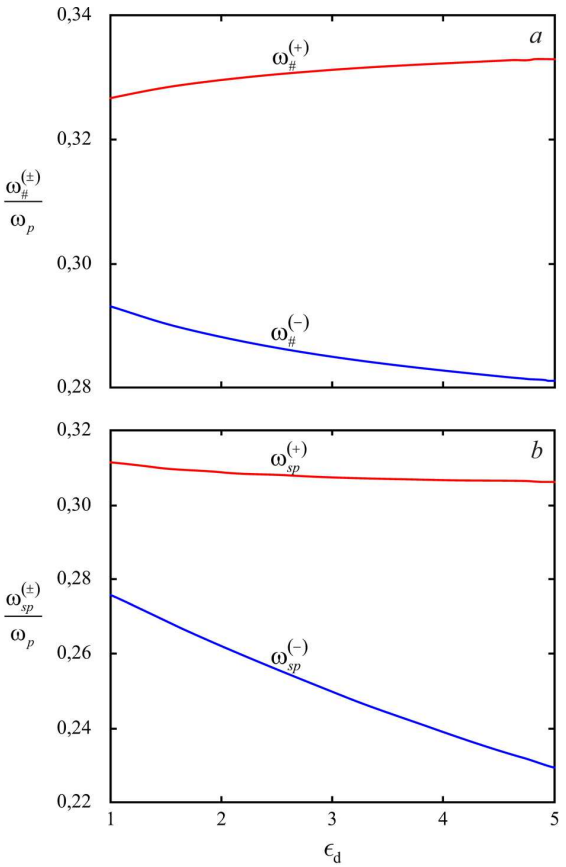

Fig. 6. Dependences of the upper and lower branches of (*a*) the invisibility frequencies and (*b*) the SPR frequencies on the substrate dielectric permittivity for Au hemispheres

solute values of the extrema in the Pt case are larger, and the second maximum of the imaginary part is more pronounced. This is a result of a substantial difference between the values of the optical parameters for these materials.

In Fig. 5, *a*, the frequency dependences of the imaginary part of the polarization for hemispherical nanoislands of various metals with the radius $R = 20$ nm are exhibited. It is interesting that the second maximum for Au or Cu nanoislands is weakly pronounced, in contrast to Ag, Pd, and Pt islands with the same radius. This is also a result of a substantial difference between the frequencies of bulk plasmons and the contributions of the crystal lattice to the dielectric permittivity.

The frequency dependences of the imaginary part of the transverse component of the polarizability tensor for Au nanoislands on a glass substrate and in various environments are shown in Fig. 5, *b*. The results of calculations demonstrate that as $\epsilon_{\rm m}$ increases, the maximum values of $\mathrm{Im}\,\tilde{\alpha}_{\rm q}^{\perp}$ and the distance between the first and second maxima also increase, whereas the difference between the maximum values decreases, i.e., the amplitude of the second maximum approaches the amplitude of the first maximum. This occurs, because the quadrupole contribution to the polarizability becomes comparable to the dipole one.

Figure 5, *c* demonstrates analogous curves for Al islands with $R = 20$ nm and for various effective electron masses. One can see that the effective-mass reduction gives rise to a "blue" shift of the frequency

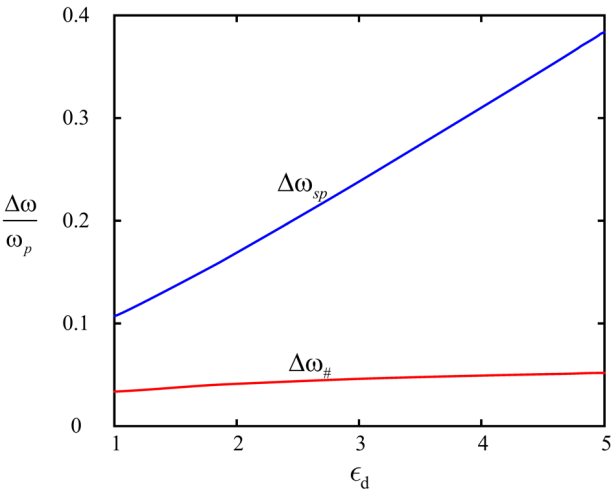

Fig. 7. Dependences of the SPR and invisibility frequency differences on the substrate dielectric permittivity for Au hemispheres

maxima in the imaginary part of the polarizability, because the frequency of bulk plasmons and, therefore, the SPR frequency decrease in this case. It should also be noted that the peaks are sharp and their broadening is small, which testifies that the effective relaxation time in Al islands is longer than in islands of other metals.

The dependences of the invisibility and SPR frequencies on the substrate dielectric permittivity $\epsilon_{\rm d}$ are shown in Fig. 6. It follows from Eqs. (26) and (31) that a hemispherical island has two invisibility frequencies $\omega_{\#}^{(\pm)}$ and two SPR frequencies $\omega_{sp}^{(\pm)}$, i.e., the splitting of the invisibility and SPR frequencies takes place. Note that the invisibility frequency $\omega_{\#}^{(+)}$ weakly increases, whereas the invisibility frequency $\omega_{\#}^{(-)}$ slightly decreases with the growth of the substrate dielectric permittivity (Fig. 6, *a*). At the same time, the SPR frequency $\omega_{sp}^{(+)}$ decreases weakly and the SPR frequency $\omega_{sp}^{(-)}$ decreases strongly, as $\epsilon_{\rm d}$ grows (Fig. 6, *b*).

Regarding the splitting magnitudes of the invisibility frequencies, $\Delta\omega_{\#}$, and the SPR frequencies, $\Delta\omega_{sp}$, it is worth noting (Fig. 7) that the difference $\Delta\omega_{\#}$ increases very weakly with the growth of the substrate dielectric permittivity; on the contrary, the splitting $\Delta\omega_{sp}$ increases substantially. Thus, for the formation of an "invisibility" frequency band, it is necessary to use substrates with the dielectric permeability as low as possible.

4. Conclusions

The electrostatic problem of determining the potential in the system "a hemispherical metal nanoparticle on a dielectric substrate" has been solved in the quasistatic quadrupole approximation. The frequency dependences of the transverse component of the polarizability tensor and expressions for the invisibility and SPR frequencies are obtained taking the dipole and quadrupole contributions into account.

It is shown that the growth of the nanoparticle radius R makes plasmon resonances more pronounced, with the second resonance appearing at $R \approx 20$ nm. The presence of two resonances can be explained by the excitation of the dipole and quadrupole modes of the surface plasmon resonance.

Owing to different bulk plasmon frequencies, as well as crystal-lattice contributions, the second maximum in the imaginary part of the polarizability for Ag, Pd, and Pt islands is more pronounced than that for Au and Cu islands.

The peaks in the frequency dependences of the imaginary part of the polarization for Al islands are sharp, and their broadening is low because of the long relaxation time and the small value of ϵ^{∞}. As a result, a substantial splitting of the surface plasmon resonance takes place.

It is found that, for the formation of an "invisibility band" in some space region in the immediate vicinity of the metal nanoisland, substrates made of materials with the lowest values of dielectric permittivity should be used.

APPENDIX

Expressions for the frequency dependence pof olarizability accounting for the dipole and quadrupole contributions

From the boundary conditions (3) at $\theta = \frac{\pi}{2}$, it follows that

$$\begin{cases} A_1 = D_1; \\ B_1 = C_1; \\ \epsilon(\omega) A_2 = \epsilon_d D_2; \\ \epsilon_d B_2 = \epsilon_m C_2. \end{cases} \tag{A.1}$$

In order to apply the boundary conditions at the spherical surface ($r = R$), let us multiply each term in expressions (15)–(18) by $\sin\theta P_2^1(\cos\theta)$ and integrate the results over θ in the upper half-plane from 0 to $\frac{\pi}{2}$, and in the lower one from $\frac{\pi}{2}$ to π. In view of formulas (19) and (20), we obtain

$$\int\limits_0^{\frac{\pi}{2}} \sin\theta P_1^1(\cos\theta) P_2^1(\cos\theta)\, d\theta = 3 \int\limits_0^{\frac{\pi}{2}} \sin^3\theta \cos\theta d\theta =$$

$$= 3\int\limits_0^{\frac{\pi}{2}} \sin^3\theta d\left(\sin\theta\right) = \frac{3}{4};$$

$$\int\limits_0^{\frac{\pi}{2}} \sin\theta \left[P_2^1\left(\cos\theta\right)\right]^2 d\theta = 9\int\limits_0^{\frac{\pi}{2}} \sin^3\theta\cos^2\theta d\theta =$$

$$= -9\int\limits_0^{\frac{\pi}{2}} \left(1-\cos^2\theta\right)\cos^2\theta d\left(\cos\theta\right) = \frac{6}{5};$$

$$\int\limits_{\frac{\pi}{2}}^{\pi} \sin\theta P_1^1\left(\cos\theta\right) P_2^1\left(\cos\theta\right) d\theta = 3\int\limits_{\frac{\pi}{2}}^{\pi} \sin^3\theta\cos\theta d\theta$$

$$= 3\int\limits_{\frac{\pi}{2}}^{\pi} \sin^3\theta d\left(\sin\theta\right) = -\frac{3}{4};$$

$$\int\limits_{\frac{\pi}{2}}^{\pi} \sin\theta \left[P_2^1\left(\cos\theta\right)\right]^2 d\theta = 9\int\limits_{\frac{\pi}{2}}^{\pi} \sin^3\theta\cos^2\theta d\theta$$

$$= -9\int\limits_{\frac{\pi}{2}}^{\pi} \left(1-\cos\theta\right)\cos^2\theta d\left(\cos\theta\right) = \frac{6}{5}.$$

Therefore,

$$\varphi_1 = \int\limits_0^{\frac{\pi}{2}} \varphi_1\left(r,\theta,\phi\right)\sin\theta P_2^1\left(\cos\theta\right) d\theta =$$

$$= \left[\frac{3}{4}A_1 r + \frac{6}{5}A_2 r^2\right]\cos\phi;$$

$$\varphi_2 = \int\limits_{\frac{\pi}{2}}^{\pi} \varphi_2\left(r,\theta,\phi\right)\sin\theta P_2^1\left(\cos\theta\right) d\theta =$$

$$= \left[-\frac{3}{4}\frac{B_1}{r^2} + \frac{6}{5}\frac{B_2}{r^3} + \frac{3}{4}\mathcal{E}_0 r\right]\cos\phi;$$

$$\varphi_3 = \int\limits_{\frac{\pi}{2}}^{\pi} \varphi_3\left(r,\theta,\phi\right)\sin\theta P_2^1\left(\cos\theta\right) d\theta =$$

$$= \left[\frac{3}{4}\frac{C_1}{r^2} + \frac{6}{5}\frac{C_2}{r^3} + \frac{3}{4}\mathcal{E}_0 r\right]\cos\phi;$$

$$\varphi_4 = \int\limits_{\frac{\pi}{2}}^{\pi} \varphi_4\left(r,\theta,\phi\right)\sin\theta P_2^1\left(\cos\theta\right) d\theta =$$

$$= \left[-\frac{3}{4}D_1 r + \frac{6}{5}D_2 r^2\right]\cos\phi.$$

Substituting these expressions into the boundary conditions (2) at the surface of the sphere, we obtain four more equations,

$$\begin{cases} \dfrac{3}{4}A_1 R + \dfrac{6}{5}A_2 R^2 = \dfrac{3}{4}\dfrac{C_1}{R^2} + \dfrac{6}{5}\dfrac{C_2}{R^3} - \dfrac{3}{4}\mathcal{E}_0 R, \\ -\dfrac{3}{4}\dfrac{B}{R^2} + \dfrac{6}{5}\dfrac{B_2}{R^3} + \dfrac{3}{4}\mathcal{E}_0 R = -\dfrac{3}{4}D_1 R + \dfrac{6}{5}D_2 R^2, \\ -\dfrac{3}{4}D_1 + \dfrac{12}{5}D_2 R = \dfrac{3}{2}\dfrac{B_1}{R^3} - \dfrac{18}{5}\dfrac{B_2}{R^4} + \dfrac{3}{4}\mathcal{E}_0, \\ \epsilon\left(\omega\right)\left[\dfrac{3}{4}A_1 + \dfrac{12}{5}A_2 R\right] = \epsilon_m\left[-\dfrac{3}{2}\dfrac{C_1}{R^3} - \dfrac{18}{5}\dfrac{C_2}{R^4} - \dfrac{3}{4}\mathcal{E}_0\right]. \end{cases} \tag{A.2}$$

Relations (A.1) and (A.2) compose a system of eight equations for eight unknowns: $A_{1,2}$, $B_{1,2}$, $C_{1,2}$, and $D_{1,2}$. By determining the quantity C_1 and substituting it into the expression

$$\tilde{\alpha} = \frac{C_1}{2R^3\mathcal{E}_0}$$

for the dimensionless polarizability, we arrive at formulas (21)–(23).

1. U. Kreibig, M. Vollmer. *Optical Properties of Metal Clusters* (Springer, 1995) [ISBN: 978-0471524175].
2. S.A. Maier. *Plasmonics: Fundamentals and Applications* (Springer, 2007) [ISBN: 978-0-387-37825-1].
3. M.L. Brongersma, V.M. Shalaev. Applied physics. The case for plasmonics. *Science* **328**, 440 (2010).
4. J.A. Schuller, E.S. Barnard, W. Cai, Y.Ch. Jun, J.S. White, M.L. Brongersma. Plasmonics for extreme light concentration and manipulation. *Nat. Mater.* **9**, 193 (2010).
5. V.V. Klimov. *Nanoplasmonics* (CRC Press, 2014) [ISBN: 978-9814267168].
6. M.L. Dmytruk, S.Z. Malynych. Surface plasmon resonances and their manifestation in the optical properties of noble-metal nanostructures. *Ukr. Fiz. Zh. Ogl.* **9**, 3 (2014) (in Ukrainian).
7. D.J. De Aberasturi, A.B. Serrano-Montes, L.M. Liz-Marzán. Modern applications of plasmonic nanoparticles: from energy to health. *Adv. Opt. Mater.* **3**, 602 (2015).
8. *Handbook of Surface Plasmon Resonance.* Edited by R.B.M. Schasfoort (RSC Publishing, 2017) [ISBN: 978-1-78262-730-2].
9. A.O. Koval, A.V. Korotun, Yu.A. Kunytskyi, V.A. Tatarenko, I.M. Titov. *Electrodynamics of Plasmon Effects in Nanomaterials* (Naukova Dumka, 2021) (in Ukrainian) [ISBN: 978-966-00-1761-0].
10. C.F. Bohren, D.R. Huffman. *Absorption and Scattering of Light by Small Particles* (Wiley, 1998) [ISBN: 9783527618156].
11. K.L. Kelly, E. Coronado, L.L. Zhao, G.C. Schatz. The optical properties of metal nanoparticles: the influence of size, shape, and dielectric environment. *J. Phys. Chem. B* **107**, 668 (2003).

12. N.I. Grigorchuk, P.M. Tomchuk. Cross-sections of electric and magnetic light absorption by spherical metallic nanoparticles. The exact kinetic solution. *Ukr. J. Phys.* **51**, 921 (2006).
13. N.I. Grigorchuk. Plasmon resonant light scattering on spheroidal metallic nanoparticle embedded in a dielectric matrix. *Europhys. Lett.* **97**, 45001 (2012).
14. V.A.G. Rivera, F.A. Ferri, E. Marega. Localized surface plasmon resonances: noble metal nanoparticle interaction with rare-earth ions. *Plasm. Princ. App.* **11**, 283 (2012).
15. K.M. Mayer, J.H. Hafner. Localized surface plasmon resonance sensors. *Chem. Rev.* **111**, 3828 (2011).
16. D. Dini, M.J.F. Calvete, M. Hanack. Nonlinear optical materials for the smart filtering of optical radiation. *Chem. Rev.* **116**, 13043 (2016).
17. A.V. Korotun, A.O. Koval, A.A. Kryuchyn, V.M. Rubish, V.V. Petrov, I.M. Titov. *Nanophotonic Technologies. Current State and Prospects* (FOP Sabov A.M., 2019) (in Ukrainian).
18. D. Pineda-Vázquez, A.J. Polanco-Mendoza, G. Morales-Luna, A. Rodríguez-Gómez, A. Reyes-Coronado, G. Pirruccio, A. García-Valenzuela, R.G. Barrera. Internal reflectance from a disordered monolayer of small gold nanoparticles on a glass substrate: Theory vs. experiment. *Mater. Today Proc.* **13**, 404 (2019).
19. T. Chung, Y. Lee, M.-S. Ahn, W. Lee, S.-In Bae, C. Hwang, K.-H. Jeong. Nanoislands as plasmonic materials. *Nanoscale* **11**, 8651 (2019).
20. P.M. Tomchuk, V.N. Starkov. Electron-lattice energy exchange and hot electrons in metal island films. *Ukr. J. Phys.* **65**, 973 (2020).
21. M. Held, O. Stenzel, S. Wilbrandt, N. Kaiser, A. Tunnermann. Manufacture and characterization of optical coatings with incorporated copper island films. *Appl. Optics* **51**, 4436 (2012).
22. K. Aslan, S.N. Malyn, C.D. Geddes. Angular-dependent metal-enhanced fluorescence from silver island films. *Chem. Phys. Lett.* **453**, 222 (2008).
23. T.R. Jensen, R.P. Van Duyne, S.A. Johnson, V.A. Maroni. Surface-enhanced infrared spectroscopy: a comparison of metal island films with discrete and non-discrete surface plasmons. *Appl. Spectrosc.* **54**, 371 (2000).
24. P. Heger, O. Stenzel, N. Kaiser. Metal island films for optics. *Proc. SPIE* **5250**, 21 (2004).
25. M. Subr, M. Petr, O. Kylian, J. Kratochvil, J. Prochazka. Large-scale Ag nanoislands stabilized by a magnetron-sputtered polytetrafluoroethylene film as substrates for highly sensitive and reproducible surface-enhanced Raman scattering (SERS). *J. Mater. Chem. C* **3**, 11478 (2015).
26. M.A. Badshah, N.Y. Koh, A.W. Zia, N. Abbas, Z. Zahra, M.W. Saleem. Recent developments in plasmonic nanostructures for metal enhanced fluorescence-based biosensing. *Nanomater.* **10**, 1749 (2020).
27. G. Min, Z. Qiming, L. Simone. Nanomaterials for optical data storage. *Nat. Rev. Mater.* **1**, 16070 (2016).
28. V.V. Petrov, A.A. Kryuchyn, V.M. Rubish, M.L. Trunov. Recording of micro/nanosized elements on thin films of glassy chalcogenide semiconductors by optical radiation. In: *Chalcogenides – Preparation and Applications* (IntechOpen, 2022), 176 p.
29. S. Malynych, G. Chumanov. Light-induced coherent interactions between silver nanoparticles in two-dimensional arrays. *J. Am. Chem. Soc.* **125**, 2896 (2003).
30. M. Kang, J.J. Kim, Y.J. Oh, S.G. Park, K.H. Jeong. A deformable nanoplasmonic membrane reveals universal correlations between plasmon resonance and surface enhanced raman scattering. *Adv. Mater.* **26**, 4510 (2014).
31. P.M. Tomchuk, B.P. Tomchuk. Optical absorption by small metal particles. *Zh. Èksp. Teor. Fiz.* **112**, 661 (1997) (in Russian).
32. R.D. Fedorovich, A.G. Naumovets, P.M. Tomchuk. Electron and light emission from island metal films and generation of hot electrons in nanoparticles. *Phys. Rep.* **328**, 73 (2000).
33. P.M. Tomchuk, N.I. Grigorchuk. Shape and size effects on the energy absorption by small metallic particles. *Phys. Rev. B* **73**, 155423 (2006).
34. N.I. Grigorchuk. Radiative damping of surface plasmon resonance in spheroidal metallic nanoparticle embedded in a dielectric medium. *J. Opt. Soc. Am. B* **29**, 3404 (2012).
35. N.I. Grigorchuk. Broadening of surface plasmon resonance line in spheroidal metallic nanoparticles. *J. Phys. Stud.* **20**, 1701 (2016).
36. A.V. Korotun, N.I. Pavlyshche. Cross sections for absorption and scattering of electromagnetic radiation by ensembles of metal nanoparticles of different shapes. *Phys. Met. Metallogr.* **122**, 941 (2021).
37. A.V. Korotun, Ya.V. Karandas, V.I. Reva, I.M. Titov. Polarizability of two-layer metal-oxide nanowires. *Ukr. J. Phys.* **66**, 906 (2021).
38. A.V. Korotun, A.A. Koval', V.I. Reva, I.N. Titov. Optical absorption of a composite based on bimetallic nanoparticles. Classical approach. *Phys. Met. Metallogr.* **120** 1040 (2019).
39. A.V. Korotun, A.A. Koval'. Optical properties of spherical metal nanoparticles coated with an oxide layer. *Opt. Spectrosc.* **127** 1161 (2019).
40. V. Zhurikhina, P. Brunkov, V. Melehin, T. Kaplas, Y. Svirko, V. Rutckaia, A. Lipovskii. Self-assembled silver nanoislands formed on glass surface via out-diffusion for multiple usages in SERS applications. *Nanoscale Res. Lett.* **7**, 676 (2012).
41. N.I. Grigorchuk, P.M. Tomchuk. Optical and transport properties of spheroidal metal nanoparticles with account for the surface effect. *Phys. Rev. B* **84**(8), 085448 (2011).
42. A.D. Yaghjian. Electric dyadic Green's functions in the source region. *Proc. IEEE* **68**, 248 (1980).
43. A.F. Nikiforov, V.B. Uvarov. *Special Functions of Mathematical Physics: A Unified Introduction with Applications* (Birkhauser, 2013).

44. A. Pinchuk, G. von Plessen, U. Kreibig. Influence of interband electronic transitions on the optical absorption in metallic nanoparticles. *J. Phys. D* **37**, 3133 (2004).

Received 04.08.22.
Translated from Ukrainian by O.I. Voitenko

А.В. Коротун

ПОЛЯРИЗОВНІСТЬ МЕТАЛЕВОЇ НАПІВСФЕРИЧНОЇ НАНОЧАСТИНКИ НА ДІЕЛЕКТРИЧНІЙ ПІДКЛАДИНЦІ

За умови нормального падіння світла на діелектричну підкладинку, у квадрупольному наближенні визначено частотну залежність дипольної поляризовності металевої півкулі, розташованої на діелектричній підкладинці. Отримано співвідношення для ефективного часу релаксації, а також для частот невидимості та поверхневого плазмонного резонансу. Досліджено еволюцію плазмонних резонансів при зміні радіусів півкуль. Обговорюються причини появи двох резонансів уявної частини поляризовності та відмінностей величини максимумів уявної частини поляризовності півкуль різних металів. Пояснюється характер і положення резонансів уявної частини поляризовності для острівців алюмінію. Наводяться рекомендації стосовно створення частотної смуги невидимості поблизу металевого наноострівця.

Ключові слова: металева півкуля, поляризовність, поверхневий плазмонний резонанс, частота невидимості, квадрупольне наближення.